

A Data-centric Supervised Transfer Learning Framework for DOA Estimation with Array Imperfections

Bo Zhou, Kaijie Xu, Yinghui Quan and Mengdao Xing, *Fellow, IEEE*

Abstract—In practical scenarios, processes such as sensor design, manufacturing, and installation will introduce certain errors. Furthermore, mutual interference occurs when the sensors receive signals. These defects in array systems are referred to as array imperfections, which can significantly degrade the performance of Direction of Arrival (DOA) estimation. In this study, we develop a deep-learning based transfer learning approach, which effectively mitigates the degradation of deep-learning based DOA estimation performance caused by array imperfections. In this study, we develop a novel deep learning-based transfer learning method that effectively counteracts the negative impact of array imperfections on data-driven DOA estimation performance. In the developed scheme, we highlight three major contributions. First, we propose a Vision Transformer based method for DOA estimation, which achieves excellent performance in scenarios with low signal-to-noise ratios and limited snapshots. Second, we introduce a transfer learning framework that extends deep learning models from ideal simulation scenarios to complex real-world scenarios with array imperfections. By leveraging only conventional simulation data, the proposed transfer learning framework significantly enhances the performance of existing DOA estimation algorithms under array defects, without the need for large amounts of real-world data. Finally, we incorporate visualization and evaluation metrics to assess the performance of DOA estimation methods, which allow for a more thorough evaluation of methods and further validate the developed framework. Our code can be accessed at <https://github.com/zzb-nice/DOA est Master>.

Index Terms—Direction of Arrival (DOA) estimation, Array Imperfections, Vision Transformer, Domain Adaptation, Data-centric Methods.

I. INTRODUCTION

Direction of Arrival (DOA) estimation finds extensive applications across various engineering fields, including wireless communications, astronomical observation, radar, and sonar [2][3], where accurately determining the direction of incoming signals is crucial for efficient operation. Nowadays, as radar technology becomes increasingly accessible for civilian use, DOA estimation methods have also been applied in emerging areas such as

This research is supported by the National Natural Science Foundation of China (Nos. 62101400, 72101075, 72171069 and 92367206), and in part by the Shaanxi Fundamental Science Research Project for Mathematics and Physics under Grant 22JSQ032. (Corresponding author: Kaijie Xu).

autonomous driving and drone operating system [4][5].

Practical scenarios are placing higher demands on DOA estimation algorithms. For instance, in autonomous driving scenarios, there is an increasing need for DOA estimation of fast-moving small targets [4]. In non-cooperative target localization scenarios, it is essential to achieve rapid and precise DOA estimation [6][7]. These practical scenarios generally require accurate DOA estimation results under conditions of low Signal-to-Noise Ratios (SNR) and small snapshots, along with high real-time performance. This highlights the urgent need for efficient estimation methods with relatively low computational complexity, capable of delivering high accuracy under ideal conditions while also exhibiting resilience in low SNR and small-sample settings.

Over the past few decades, extensive research has been conducted on DOA estimation, leading to the development of numerous algorithms [1][8–[29]. These methods can be broadly categorized into model-driven and data-driven approaches. Among them, model-driven methods have been more extensively studied due to their well-established theoretical foundations. Based on different estimation strategies, model-driven approaches can be further classified into several major categories, including beamforming methods [8], subspace methods [9]–[12], maximum likelihood methods [13]–[15], and compressed sensing (sparsity-inducing) methods [16]–[19].

A leading and well-respected family of model-driven approaches is the subspace method, which achieves satisfactory performance in scenarios with high SNR and large snapshots. This method maintains relatively low computational complexity when a limited number of array elements is used. However, its performance deteriorates significantly in practical scenarios with low SNR and small snapshots. While compressive sensing-based and maximum likelihood-based methods have yielded notable improvements, they remain constrained by real-time performance limitations. Consequently, model-driven methods for DOA estimation have reached a performance bottleneck in practical scenarios.

Machine learning and deep learning methods have emerged as prominent methods for DOA estimation in recent years.

Bo Zhou, Kaijie Xu and Yinghui Quan are with the School of Information Mechanics and Sensing Engineering, Xidian University, Xi'an 710071, China (e-mail: 23021211623@stu.xidian.edu.cn; kjxu@xidian.edu.cn; yhquan@mail.xidian.edu.cn). Mengdao Xing is with the National Laboratory of Radar Signal Processing, Xidian University, Xi'an 710071, China (email: xmd@xidian.edu.cn).

These methods build complex mapping relationships from input to output based on large-scale datasets. Unlike model-driven methods that rely on predefined signal models, data-driven methods generally do not impose prior assumptions on the input and output. This makes them particularly suitable for practical scenarios where the signal model may be incomplete or inaccurate. Furthermore, during practical implementation, data-driven methods demonstrate better real-time performance due to their fast inference speed. As a result, data-driven methods are considered promising tools for DOA estimation in practical scenarios.

Deep learning methods are first introduced to address the problem of DOA estimation in the 1990s [20][21]. Recent advancements in computational hardware [30] have been a key driver behind the accelerated development of data-driven approaches. The investigations conducted in [1][22] pioneer the implementation of Deep Neural Network (DNN) and Convolutional Neural Network (CNN) for DOA estimation. Subsequently, the methods proposed in [23][24] advance the field by initially partitioning the incoming signal into multiple sub-regions using a network architecture, and then deploying parallel networks to process these sub-regions independently.

Moreover, some studies focus on combining traditional DOA estimation (model-driven) techniques with deep learning (data-driven) approaches. The inherent flexibility of deep learning methods enables the modeling of diverse and complex mappings, which facilitates their effective integration with classical methods. The method proposed in [25][26] integrate subspace-based methods with deep neural networks. Specifically, a CNN is employed to reconstruct a noise-free covariance matrix, after which a classical subspace-based approach is applied for DOA estimation. Similarly, the approaches in [27][28] combine deep learning with compressed sensing algorithms. Furthermore, Shmuel et al. [29] introduce SubspaceNet, which utilizes the differentiability of polynomial equation root-finding and matrix decomposition; thereby directly treating the Root-MUSIC algorithm as part of the network.

Nevertheless, most of the model-driven and data-driven methods mentioned above do not account for array imperfections in practical systems. The existence of array position biases, amplitude and phase inconsistencies, as well as mutual coupling effects [31] can affect the DOA estimation accuracy of models. Such imperfections often substantially impair the model's DOA estimation capability, potentially leading to complete failure.

A series of active calibration [32]–[36] and self-calibration [37]–[43] methods have been applied to compensate for array imperfections in practical scenarios. Among them, active calibration methods require the setup of known signal sources with predefined DOA directions, which are specifically employed for the compensation of array imperfections. In contrast, self-calibration methods do not require additional auxiliary signal sources and can dynamically calibrate the array imperfections during array system applications, offering significant practical advantages. However, self-calibration

methods generally estimate array imperfections simultaneously with DOA values, often relying on initialization and struggling to handle more severe array imperfections. As highlighted in [37], most existing self-calibration methods perform well only under relatively ideal signal conditions, while they struggle in practical scenarios characterized by low SNR, limited snapshots, and closely spaced sources. These conditions present significant challenges for many DOA estimation algorithms.

Moreover, existing calibration methods are constrained by numerous limitations. Due to the significant difficulty in directly modeling and analyzing all array imperfections, most existing calibration algorithms can focus on only one of the array imperfections, such as array position biases [32][35][36], amplitude-phase inconsistencies [38]–[40] or mutual coupling [41]–[43]. Only a few studies explore how to address scenarios involving multiple array imperfections [33][34][37]. Some methods are even limited to specific array structures, such as uniform linear or circular arrays [40][41], or rely on additional assumptions to simplify the model [37]. Therefore, how to effectively address scenarios with multiple array imperfections remains an issue that requires further exploration.

Based on the simulation results, it can be observed that in scenarios with low SNR and small snapshots, deep learning models remain sensitive to array imperfections, requiring the application of calibration models to compensate for array imperfections. However, along with the development of deep learning technologies, it is possible to directly construct a transfer learning algorithm [44] that transitions from an ideal scenario without array imperfections to a practical scenario with array imperfections, thereby enhancing the model's adaptability to practical scenarios.

Nonetheless, there is currently a lack of research on the application of transfer learning methods for DOA estimation. To the best of our knowledge, only a few studies [45]–[47] introduce transfer learning methods into DOA estimation. The methods proposed in [45][47] migrate DOA estimation networks with a fixed number of targets to scenarios involving fewer or more targets, with the primary goal of reducing the training computational costs. In [46], Zhang et al. employ transfer learning to improve the adaptability of the constructed CNN model to array imperfections; however, they only fine-tuned the network from ideal data to data affected by array imperfections, without leveraging more advanced transfer learning strategies.

In this paper, we propose a deep learning-based supervised transfer learning framework for DOA estimation, which aims to mitigate the performance degradation of data-driven approaches in practical scenarios with various array imperfections. In the proposed approach, the data is divided into source and target domains. The source domain consists of ideal data without array imperfections, while the target domain represents practical scenarios with array imperfections. We first train a DOA estimation model using the source domain data. Then, a transfer learning technique is employed to align feature representations between the source and target domains, thereby improving the robustness of the model in challenging

conditions such as low SNR, limited snapshots, and multiple array imperfections. The main contributions of this work are as follows:

- 1) We propose a novel DOA estimation model based on Vision Transformer, which achieves outstanding performance under challenging conditions such as low SNR and limited snapshots.
- 2) To address the significant distribution shift caused by array imperfections between the source and target domains which leads to performance degradation in practical applications, we introduce a transfer learning algorithm to align feature representations and improve the generalization of the model in real-world scenarios.
- 3) Through extensive simulations, we demonstrate that the proposed method outperforms existing approaches in terms of DOA estimation accuracy and robustness.

This paper is organized as follows. Section II formulates the problem. Section III presents the design of a network for DOA estimation. Section IV introduces a transfer learning scheme for the developed model. Experimental results are given in Section V. Finally, Section VI concludes the paper.

II. PROBLEM FORMULATION

In this work, two models of array receiving signals are considered. The first is an ideal array signal model, while the second incorporates array imperfections to reflect real-world conditions.

A. Ideal Signal Model

Firstly, the ideal array reception model is constructed. Consider a Uniform Linear Array (ULA) or Uniform Circular Array (UCA) consisting of M antennas, receiving K narrowband far-field signals impinging from different DOAs. The array receiving signal model can be expressed in the following manner:

$$\begin{aligned} \mathbf{y}(t) &= \sum_{k=1}^K \mathbf{a}(\mathbf{p}, \theta_k) s_k(t) + \mathbf{n}(t) \\ &= \mathbf{A}(\mathbf{p}, \theta) \mathbf{s}(t) + \mathbf{n}(t), t = 1, \dots, T. \end{aligned} \quad (1)$$

where $\theta = [\theta_1, \dots, \theta_K]$ represents the directions of arrival, $\mathbf{A}(\mathbf{p}, \theta) = [\mathbf{a}(\mathbf{p}, \theta_1), \dots, \mathbf{a}(\mathbf{p}, \theta_K)]$ denotes the $M \times K$ array manifold matrix, and T is the number of received snapshots. $\mathbf{s}(t) = [s_1(t), \dots, s_K(t)]^T$ and $\mathbf{n}(t)$ denote the transmitted signal and the noise vector at time index t , respectively. For a ULA, $\mathbf{a}(\mathbf{p}, \theta_k)$ can be expressed as:

$$\mathbf{a}(\mathbf{p}, \theta_k) = \left[1, e^{-j\frac{2\pi d}{\lambda} \sin(\theta_k)}, \dots, e^{-j\frac{2\pi d}{\lambda} (M-1) \sin(\theta_k)} \right]^T \quad (2)$$

where $\lambda = c/f$ denotes the wavelength of the incident signals, d is the distance between the array elements, while c and f represent the propagation speed and the frequency of the incident signals, respectively. Similarly, for a UCA,

$\mathbf{a}(\mathbf{p}, \phi_k, \theta_k)$ can be represented in the following form:

$$\mathbf{a}(\mathbf{p}, \phi_k, \theta_k) = [e^{-j(2\pi/\lambda) \cos(\phi_1 - \theta_k) \sin(\phi_k)}, \dots, e^{-j(2\pi/\lambda) \cos(\phi_M - \theta_k) \sin(\phi_k)}]^T \quad (3)$$

where $\phi_m = \frac{2\pi m}{M}$ denotes the azimuth of the m th sensor of the UCA. Based on the received signal vector discussed above, the Spatial Covariance Matrix (SCM) is computed as follows:

$$\begin{aligned} R_y &= \mathbb{E}\{\mathbf{y}(t)\mathbf{y}^H(t)\} \\ &= \mathbb{E}\{\mathbf{A}(\mathbf{p}, \theta) \mathbf{s}(t) \mathbf{s}^H(t) \mathbf{A}^H(\mathbf{p}, \theta)\} + \mathbb{E}\{\mathbf{n}(t) \mathbf{n}^H(t)\} \\ &= \mathbf{A}(\mathbf{p}, \theta) \mathbf{R}_s \mathbf{A}^H(\mathbf{p}, \theta) + \sigma_N^2 \mathbf{I}_M \end{aligned} \quad (4)$$

where $\mathbb{E}\{\cdot\}$ denotes the expectation operator, $\mathbf{R}_s = \mathbb{E}\{\mathbf{s}(t)\mathbf{s}^H(t)\}$ represents the covariance matrix of incident signals and σ_N^2 stands for the noise power. However, since the number of snapshots is limited in practice, the SCM is replaced by the sampled SCM calculated via:

$$\tilde{\mathbf{R}}_y = \frac{1}{T} \sum_{t=1}^T \mathbf{y}(t) \mathbf{y}^H(t) \quad (5)$$

$\tilde{\mathbf{R}}_y$ is an unbiased estimate of \mathbf{R}_y calculated by the received signal vector. Most existing DOA estimation algorithms focus on deriving the source DOAs $\theta = [\theta_1, \dots, \theta_K]$ from the sampled SCM $\tilde{\mathbf{R}}_y$, which has been proven to be the most effective approach.

B. Signal Model with Array Imperfection

In practical applications, the array signal reception model often deviates from its theoretical ideal. Position errors can occur during the placement of array elements, while amplitude and phase inconsistencies may arise from sensor design and manufacturing defects. Additionally, mutual coupling effects can be introduced during signal reception. In [23], Liu et al. establish a simplified model to show how these three array imperfections affect the signal model in ULA, and introduce a hyperparameter $\rho \in [0, 1]$ to succinctly control the intensity of these array imperfections. The calculation of relevant parameters is as follows:

$$\begin{aligned} \mathbf{e}_{\text{pos}} &= \rho \times [0, -0.2, \dots, -0.2, 0.2, 0.2, \dots, 0.2]^T \times d \\ \mathbf{e}_{\text{gain}} &= \rho \times [0, 0.2, \dots, 0.2, -0.2, \dots, -0.2]^T \\ \mathbf{e}_{\text{phase}} &= \rho \times [0, -30^\circ, \dots, -30^\circ, 30^\circ, \dots, 30^\circ]^T \\ \mathbf{e}_{\text{mc}} &= \rho \times [\gamma^0, \gamma^1, \dots, \gamma^{M-1}]^T \end{aligned} \quad (6)$$

where $\gamma = 0.3e^{j60^\circ}$ is the mutual coupling coefficient between adjacent sensors. The term \mathbf{e}_{pos} represents the positional bias of each array element, while \mathbf{e}_{gain} and $\mathbf{e}_{\text{phase}}$ denote the amplitude and phase biases, respectively. \mathbf{e}_{mc} models the magnitude of the mutual coupling effect for a ULA, with the coupling strength proportional to the square of the distance between elements. The matrix \mathbf{E}_{mc} , denoted as a Toeplitz matrix with parameter vector \mathbf{e}_{mc} [48], can be employed to

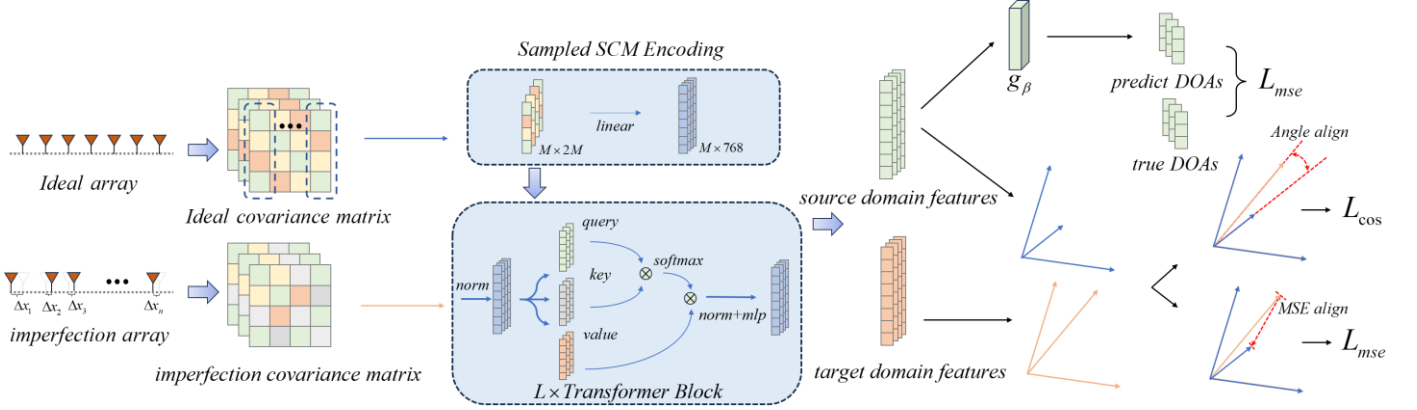


Fig. 1. The framework of DOA-ViT and transfer learning approach proposed for array imperfections.

model the mutual coupling across the entire array:

$$\mathbf{E}_{mc} = \begin{bmatrix} \gamma^0 & \gamma^1 & \dots & \gamma^i & \gamma^{i+1} & \dots & \gamma^{M-1} \\ \gamma^1 & \gamma^0 & \gamma^1 & \dots & \gamma^i & \dots & \vdots \\ \vdots & \gamma^1 & \gamma^0 & \ddots & \dots & \ddots & \vdots \\ \gamma^i & \dots & \ddots & \ddots & \ddots & \ddots & \gamma^i \\ \gamma^{i+1} & \ddots & \dots & \ddots & \ddots & \ddots & \vdots \\ \vdots & \ddots & \ddots & \dots & \ddots & \gamma^0 & \gamma^1 \\ \gamma^{M-1} & \dots & \gamma^{i+1} & \gamma^i & \dots & \gamma^1 & \gamma^0 \end{bmatrix} \quad (7)$$

Similarly, for a UCA, the \mathbf{e}_{mc} is exponentially related to the inter-element spacing. The position bias \mathbf{e}_{pos} can be extended to both the x and y -axes, while \mathbf{e}_{gain} and \mathbf{e}_{phase} remain unchanged. The steering vector affected by all three array imperfections can be expressed as:

$$\mathbf{a}(\theta, \mathbf{e}) = (\mathbf{I}_M + \delta_{mc} \mathbf{E}_{mc}) \times (\mathbf{I}_M + \text{Diag}(\delta_{gain} \mathbf{e}_{gain}) \times \text{Diag}(\exp(j\delta_{phase} \mathbf{e}_{phase})) \times \mathbf{a}(\theta, \mathbf{p} + \delta_{pos} \mathbf{e}_{pos}) \quad (8)$$

where $\delta(\cdot)$ is used to denote specific array imperfections, \mathbf{I}_M represents the $M \times M$ identity matrix, while $\text{Diag}(\cdot)$ denotes a diagonal matrix formed from a given vector. And $\mathbf{a}(\theta, \mathbf{p} + \mathbf{e}_{pos})$ refers to the array steering vector obtained based on the position biases:

$$\mathbf{a}(\theta_k, \mathbf{p} + \mathbf{e}_{pos}) = \left[e^{-j\frac{2\pi}{\lambda}(0d + e_{pos}^0) \sin(\theta_k)}, e^{-j\frac{2\pi}{\lambda}(1d + e_{pos}^1) \sin(\theta_k)}, \dots, e^{-j\frac{2\pi}{\lambda}((N-1)d + e_{pos}^{N-1}) \sin(\theta_k)} \right]^T \quad (9)$$

where \mathbf{e}_{pos}^i represents the position biases of the i th antenna. The final result $\mathbf{a}(\theta, \mathbf{e})$ in (8) represents the steering vector influenced by the three types of array imperfections. Therefore, the imperfection steering matrix \mathbf{A} can be expressed in the following form:

$$\mathbf{A}(\theta, \mathbf{e}) = [\mathbf{a}(\theta_1, \mathbf{e}), \mathbf{a}(\theta_2, \mathbf{e}), \dots, \mathbf{a}(\theta_K, \mathbf{e})] \quad (10)$$

By substituting $\mathbf{A}(\theta, \mathbf{e})$ for the steering matrix $\mathbf{A}(\mathbf{p}, \theta)$ in Section II-A, a more accurate simulation of the array signal reception model in practical scenarios can be achieved.

III. FRAMEWORK OF DOA-VIT AND TRANSFER LEARNING

Given the remarkable performance of the Vision Transformer (ViT) model across various domains, its strong nonlinear representation capability and efficient feature learning ability are expected to enhance subsequent transfer learning. Therefore, we adopt ViT as the backbone of our model. The overall architecture, referred to as DOA-ViT, is illustrated in Fig. 1. In terms of model design, we adhere to the original ViT framework [49] as closely as possible to ensure consistency and leverage its proven architecture.

A. Covariance Matrix Embedding

Since the transformer encoder can only operate on a set of input vectors, it is necessary to encode the input covariance matrix into a set of vectors. To achieve this, the split and vectorization operation is implemented, which is detailed in (11) and (12). The sampled SCM $\tilde{\mathbf{R}}_y$ is partitioned column-wise into M smaller blocks and subsequently each block is flattened into a vector of size $2M$, resulting in M vectors. Finally, a linear layer is utilized to encode each input vector, generating a matrix of dimensions $M \times D$, which represents M vectors. Each of dimension D are described in the following form:

$$\tilde{\mathbf{R}}_y = [\mathbf{r}_1, \mathbf{r}_2, \mathbf{r}_3, \dots, \mathbf{r}_M], \tilde{\mathbf{R}}_y \in \mathbb{C}^{M \times M}, \mathbf{r}_i \in \mathbb{C}^M \quad (11)$$

$$\tilde{\mathbf{r}}_i = [\text{real}(\mathbf{r}_i); \text{imag}(\mathbf{r}_i)], \tilde{\mathbf{r}} \in \mathbb{R}^{2M} \quad (12)$$

$$\mathbf{x}_i = \mathbf{E} \tilde{\mathbf{r}}_i, \mathbf{E} \in \mathbb{R}^{D \times 2M} \quad (13)$$

$$\mathbf{X}_{\text{input}} = [\text{doa token}, \mathbf{x}_1, \mathbf{x}_2, \dots, \mathbf{x}_M] \quad (14)$$

The formulation of Covariance Matrix Embedding procedure is presented in (11) to (14). Notably, similar to the widely used transformer models, a learnable D dimensional vector, called the DOA estimation token, is added to the first column of the embedded matrix. Since the transformer encoder captures global dependencies through self-attention, the DOA estimation token effectively integrates information from the entire sequence and is subsequently used in the final task, such as classification and regression.

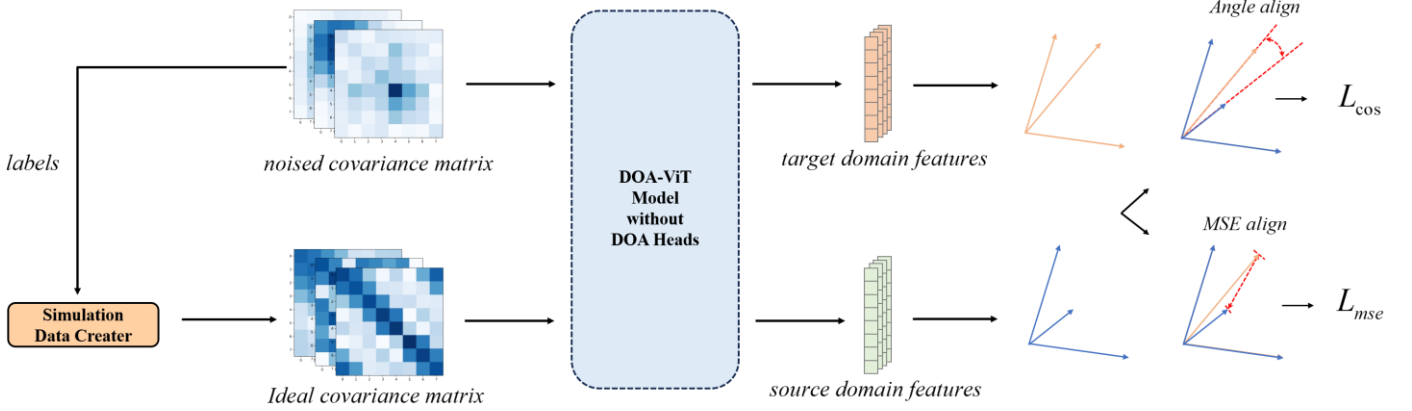


Fig. 2. The framework of transfer learning approach proposed for array imperfections.

B. Position Embedding

Transformer models inherently lack information about the order of input vectors. In other words, even if the positions of input vectors are randomly shuffled, the transformer encoder produces identical outputs for each input vector, as it treats the input vectors as an unordered set. To address this limitation, positional embeddings are introduced to encode the relative or absolute positions of the input vectors. Specifically, a set of learnable vectors, known as positional embeddings, is added directly to the input vectors as additional positional encoding information:

$$\begin{aligned} \mathbf{z}_{\text{input}} &= [\mathbf{x}_0 + \mathbf{e}_0, \mathbf{x}_1 + \mathbf{e}_1, \dots, \mathbf{x}_M + \mathbf{e}_M] \\ &= \mathbf{X}_{\text{input}} + \mathbf{E}_{\text{pos}}, \mathbf{E}_{\text{pos}} \in \mathbb{R}^{D \times (M+1)} \end{aligned} \quad (15)$$

By adding position embeddings to the input representations, the model can incorporate positional information into its computations. This mechanism is essential for tasks where understanding the sequential arrangement of input vectors significantly impacts the model's performance, such as DOA estimation.

C. Transformer Encoder

The Multi-Head Self-Attention (MHSA) mechanism is a key component of the Transformer Encoder, which is designed to enhance the capacity of the model to capture complex relationships within sequences.

Given an input $\mathbf{Z} \in \mathbb{R}^{D \times (M+1)}$, where D is the feature dimension and $M + 1$ is the sequence length, the Multi-Head Scaled-Attention (MHSA) operates as follows.

Linear Projections: The input is linearly projected into queries Q , keys K , and values V for each attention head i :

$$\mathbf{Q}_i = \mathbf{W}_i^Q \mathbf{Z}, \quad \mathbf{K}_i = \mathbf{W}_i^K \mathbf{Z}, \quad \mathbf{V}_i = \mathbf{W}_i^V \mathbf{Z}, \quad i = 1, \dots, h \quad (16)$$

where $\mathbf{W}_i^Q, \mathbf{W}_i^K, \mathbf{W}_i^V \in \mathbb{R}^{d_k \times D}$ are model parameters, and $d_k = D/h$ is the dimension of each head.

Scaled Dot-Product Attention: Each head computes attention as:

$$\text{head}_i = \text{softmax} \left(\frac{\mathbf{Q}_i \mathbf{K}_i^T}{\sqrt{d_k}} \right) \mathbf{V}_i \quad (17)$$

Concatenation and Output: The outputs of all h heads are concatenated and projected to produce the final output:

$$\text{MHSA}(\mathbf{Z}) = \mathbf{W}^O \text{Concat}(\text{head}_1, \dots, \text{head}_h) \quad (18)$$

where $\mathbf{W}^O \in \mathbb{R}^{D \times h d_k}$ is the output projection matrix. As illustrated in Fig. 1, the Transformer Encoder, consisting of layer normalization, MHSA and a Multilayer Perceptron (MLP), enables the DOA-ViT model to effectively capture and integrate global information.

D. DOA Estimation Head

The DOA Estimation Head serves as the final layer for DOA estimation. In this module, the vector corresponding to the DOA estimation token is extracted; then a linear layer is directly applied to regress the target DOA values. The loss function between the predicted DOA values and the true DOA is expressed as:

$$l(\tilde{\mathbf{R}}, \boldsymbol{\theta}; \boldsymbol{\psi}) = \min_{\mathbf{P} \in \mathcal{P}} \left(\frac{1}{K} \|\boldsymbol{\theta} - \widehat{\mathbf{P}} \tilde{\mathbf{R}}(\boldsymbol{\theta}; \boldsymbol{\psi})\|^2 \right)^{\frac{1}{2}} \quad (19)$$

where $\boldsymbol{\psi}$ represents all the parameters of the model and $\widehat{\mathbf{P}}$ is the estimation result of the DOA-ViT model, which includes K DOAs. $\boldsymbol{\theta}$ corresponds to the true DOAs, and the set \mathcal{P} encompasses all $M \times M$ permutation matrices, defined as binary matrices where each row and column contains exactly one non-zero element. The loss function for a dataset \mathcal{D} is described in the following manner:

$$\mathcal{L}_{\mathcal{D}}(\boldsymbol{\psi}) = \frac{1}{|\mathcal{D}|} \sum_{(\boldsymbol{\theta}^{(j)}, \tilde{\mathbf{R}}^{(j)}) \in \mathcal{D}} l(\tilde{\mathbf{R}}^{(j)}, \boldsymbol{\theta}^{(j)}; \boldsymbol{\psi}) \quad (20)$$

where $|\mathcal{D}|$ denotes the number of samples in the simulated dataset and $\tilde{\mathbf{R}}^{(j)}$ is the j th sampled SCM in the dataset. It is worth noting that the proposed method can be easily extended to arbitrary array configurations and Two-Dimensional (2D)

DOA estimation. If one aims to implement 2D DOA estimation, the DOA Estimation Head can be directly extended to predict the values of θ and ϕ .

IV. TRANSFER LEARNING FOR DOA ESTIMATION

By leveraging large-scale datasets for training, deep neural networks have achieved superior performance in DOA estimation. However, due to the statistical differences in the sampled SCM between simulated data and real-world data with array imperfections, the performance of the model in practical scenarios is adversely affected.

Inspired by recent advancements in transfer learning [50][51], and in order to address the significant performance degradation of deep learning models due to array imperfections in practical scenarios, we propose a supervised transfer learning approach, which is designed to enhance the adaptability of deep learning methods to array imperfections.

A. Goal of Transfer Learning

Transfer learning typically involves two tasks: the source task and the target task. The source task usually has abundant data available to effectively train the model, whereas the target task has a limited amount of data. Building on machine learning methods, transfer learning allows prior knowledge from the source task to be applied to the target task, even though there are different data distributions between the source and target tasks [44].

B. Source and Target Domains Modeling

In our transfer learning approach, two distinct scenarios are considered. The first is the ideal array signal reception scenario, which serves as a scenario that most deep learning models focus on. In this scenario, training data can typically be generated in large quantities through simulation programs, resulting in ample data availability at a relatively low cost. Consequently, deep learning algorithms can be effectively trained and validated based on the extensive dataset, ultimately achieving satisfactory performance.

The second scenario involves practical applications with array imperfections in the antenna system. In this case, data should be collected through actual measurements, resulting in higher costs and a relatively limited dataset. The ideal scenario data is treated as source domain data, and the practical scenario data as target domain data. Therefore, how to effectively leverage the prior knowledge acquired from a model trained on a substantial amount of simulation data to enhance performance of the model in a data-scarce or even data-absent practical setting becomes a valuable area for exploration.

C. Transfer learning Framework

Assume that we have already trained a model with weight parameters ψ_s that performs well on simulated data. However, in practical scenarios, array imperfections distort the statistical properties of the sampled SCM, leading to substantial statistical discrepancies between the data distributions of the source and target domains. Consequently, when applied to the target domain, the model with parameters ψ_s extracts biased features,

which in turn degrades the DOA estimation performance.

To mitigate this issue, the objective of this work is to train a feature extractor for the target domain that is designed to learn **domain-invariant features**, which remain unaffected by domain shifts induced by array imperfections and only retain the essential information relevant to the DOA estimation task, thereby enhancing the model's generalization ability in practical scenarios. The framework of our transfer learning framework is illustrated in Fig. 2, and we will provide a detailed introduction in the following.

In our transfer learning approach, we remove the DOA estimation Head from the DOA-ViT model and treat the remaining structure as a feature extractor, denoted as \mathcal{F} , which allows us to extract features from both the source and target domains:

$$\begin{aligned} \mathbf{z}_{s,i} &= \mathcal{F}_s(\tilde{\mathbf{R}}_s^{(i)}; \psi_s) \\ \mathbf{z}_{t,i} &= \mathcal{F}_t(\tilde{\mathbf{R}}_t^{(i)}; \psi_t) \end{aligned} \quad (21)$$

where \mathcal{F}_s and \mathcal{F}_t represent the feature extractors for the source and target domains, respectively, while ψ_s and ψ_t represent the model parameters for the source and target domain models. $\mathbf{z}_{s,i}$ represents the features extracted from the i th source domain input, and $\mathbf{z}_{t,i}$ denotes the features extracted from the i th target domain input.

A dataset should be constructed by collecting a series of sampled SCMs along with their corresponding DOA values in practical scenarios. Base on the true DOA values, a simulation data generator is employed to generate corresponding ideal covariance matrices that are unaffected by array imperfections, which serve as the source domain data to be aligned. As illustrated in Fig. 2, during the transfer learning approach, data in the source domain is fed into \mathcal{F}_s with frozen pre-trained weights to ensure the effectiveness of feature extraction from the source domain, while data in the target domain is fed into a trainable feature extraction module \mathcal{F}_t . In this way, by aligning the features $\mathbf{z}_{t,i}$ to $\mathbf{z}_{s,i}$, the target domain feature extractor \mathcal{F}_t can be guided to extract features that can be directly used for DOA estimation, thereby mitigating the impact of array imperfections. Two loss functions are proposed for feature alignment as follows.

MSE Loss: A mean squared error is directly applied to achieve the alignment of target domain features with source domain features.

$$\mathcal{L}_{\text{mse}}(\mathbf{z}_i^{S \leftrightarrow T}) = \|\mathbf{z}_{s,i} - \mathbf{z}_{t,i}\|^2 \quad (22)$$

where S and T represent the source and target domains, respectively. The notation $\|\cdot\|$ denotes the l_2 -norm of a vector.

Cosine Similarity Loss: To further align the structure of features between the source and target domains, we treat the features as vectors in a high-dimensional space. A cosine similarity loss is proposed to achieve angular alignment between the source domain vectors and the target domain vectors.

$$\mathcal{L}_{\text{cos}}(\mathbf{z}_i^{S \leftrightarrow T}) = \frac{\mathbf{z}_{s,i} \cdot \mathbf{z}_{t,i}}{\|\mathbf{z}_{s,i}\| \cdot \|\mathbf{z}_{t,i}\|} \quad (23)$$

where S and T represent the source and target domains, respectively. Finally, the overall loss function can be described as follows:

$$\mathcal{L}_{\text{total}}(\mathbf{Z}^S, \mathbf{Z}^T) = \alpha \mathcal{L}_{\text{cos}}(\mathbf{Z}^S, \mathbf{Z}^T) + \beta \mathcal{L}_{\text{mse}}(\mathbf{Z}^S, \mathbf{Z}^T) \quad (24)$$

where \mathbf{Z}^S and \mathbf{Z}^T represent all feature vectors extracted from the source domain and target domain, respectively, while α and β are hyper-parameters controlling the effect of the two loss functions.

Building upon the loss function of the transfer learning approach, the optimization of the target domain model parameters ψ_t is performed using first-order methods, e.g., Adaptive Moment Estimation (Adam) optimizer. To provide a more precise depiction of the overall process, the transfer learning procedure of DOA-ViT using Adam is detailed as Algorithm 1.

Algorithm 1 Transfer learning Approach using Adam

Require: DOA-ViT weights ψ_s pretrained on the source domain, hyperparameter ϵ .
Require: Target domain Dataset $\mathcal{D}_{\text{target}}$, learning rate μ , number of batches B , epochs number e_{max} .

- 1: Initialize DOA-ViT weights ψ_s for source domain model.
- 2: Initialize DOA-ViT weights ψ_t for target domain model.
- 3: **for** epoch = 0, 1, ..., e_{max} **do**
- 4: Randomly divide \mathcal{D} into B batches $\{\mathcal{D}_b\}_{b=1}^B$.
- 5: **for** $b = 1, 2, \dots, B$ **do**
- 6: **for** $(\tilde{\mathbf{R}}_b^{(j)}, \theta_b^{(j)}) \in \mathcal{D}_b$ **do**
- 7: A Simulation Data Generator creates ideal covariance matrices $\tilde{\mathbf{R}}_b^*$ based on $\theta_b^{(j)}$
- 8: Compute representations $\mathbf{Z}^S(\tilde{\mathbf{R}}_b^{(j)}, \psi_s)$ for the source domain.
- 9: Compute representations $\mathbf{Z}^T(\tilde{\mathbf{R}}_b^*, \psi_t)$ for the target domain.
- 10: **end for**
- 11: Compute $\mathcal{L}_{\mathcal{D}}(\mathbf{Z}^S, \mathbf{Z}^T)$ through Equation 24.
- 12: Update weights via $\psi_t \leftarrow \psi_t - \mu \nabla_{\psi} \mathcal{L}_{\mathcal{D}_b}(\mathbf{Z}^S, \mathbf{Z}^T)$.
- 13: **end for**
- 14: **end for**
- 15: **return** ψ_t

V. EXPERIMENTAL STUDIES

In this section, we design a series of experiments to thoroughly validate the developed scheme. Comprehensive comparisons are conducted with a wide range of classic and state-of-the-art model-driven methods, including high-resolution subspace methods such as MUSIC and Unity-ESPRIT, as well as the compressive sensing-based ℓ_1 -SVD approach, which has strong performance in low SNR and small snapshots scenarios. Additionally, we compare our method with several representative data-driven approaches and their variants

that integrate traditional algorithms developed in recent years, including the CNN-based algorithm (SPE-CNN) [1], SubspaceNet [29], ASL-2 [27], and Learning-SPICE [28]. Particular emphasis is placed on evaluating the performance of our method under non-ideal conditions, such as low signal-to-noise ratios and limited snapshots. Among these methods, SPE-CNN is recognized as a well-established deep learning-based approach, while SubspaceNet can be regarded as a subspace algorithm implemented through deep neural networks. Furthermore, ASL-2 and Learning-SPICE represent state-of-the-art techniques that integrate deep learning with compressive sensing, and are particularly designed to perform well in scenarios with a limited number of snapshots.

We begin with a detailed description of the experimental setup in Subsection V-A. The performance of the proposed model under these conditions is then presented in Subsection V-B. Furthermore, in Subsection V-C, we validate the effectiveness of transfer learning strategies through simulations conducted in practical scenarios involving array imperfections.

A. Experimental Setup

1) *Experimental scenarios*: To comprehensively evaluate the performance of the proposed algorithm, we design two representative simulation scenarios:

- *Scenario 1*: A ULA with $M = 8$ antennas and $K = 3$ signal sources. This scenario serves as a standard benchmark for multi-target DOA estimation and is widely used for performance evaluation in existing literature.
- *Scenario 2*: A UCA with $M = 12$ antennas and $K = 5$ sources. This setup is designed for two-dimensional localization tasks. It aims to assess the model's generalization capability transitioning from 1D to 2D DOA estimation.

These scenarios collectively enable a thorough assessment of the accuracy, robustness, and adaptability of the developed model across both conventional and more complex DOA estimation tasks.

2) *Hyperparameter Settings*: The proposed DOA-ViT model is configured with the following architecture and training parameters:

- The dimensionality of the embedded input vectors is set to $D = 768$, and each MHSA head has a dimension $d_k = 64$.
- The model comprises 6 stacked Transformer encoder layers, each equipped with 12 attention heads in the MHSA module.
- The feedforward neural network MLP within each encoder uses an expansion factor of 4.

For each simulation scenario, a total of 50,000 training samples and 20,000 validation samples are generated.

- In the case of a ULA, the incident angles θ are uniformly sampled from the range $[-60^\circ, 60^\circ]$ for both training and validation datasets.
- For the UCA, the azimuth angles θ are randomly generated in the range $[-180^\circ, 180^\circ]$, and the elevation angles ϕ are drawn from the range $[0^\circ, 60^\circ]$.

These settings ensure that the model is trained and validated under diverse conditions, enabling accurate DOA estimation

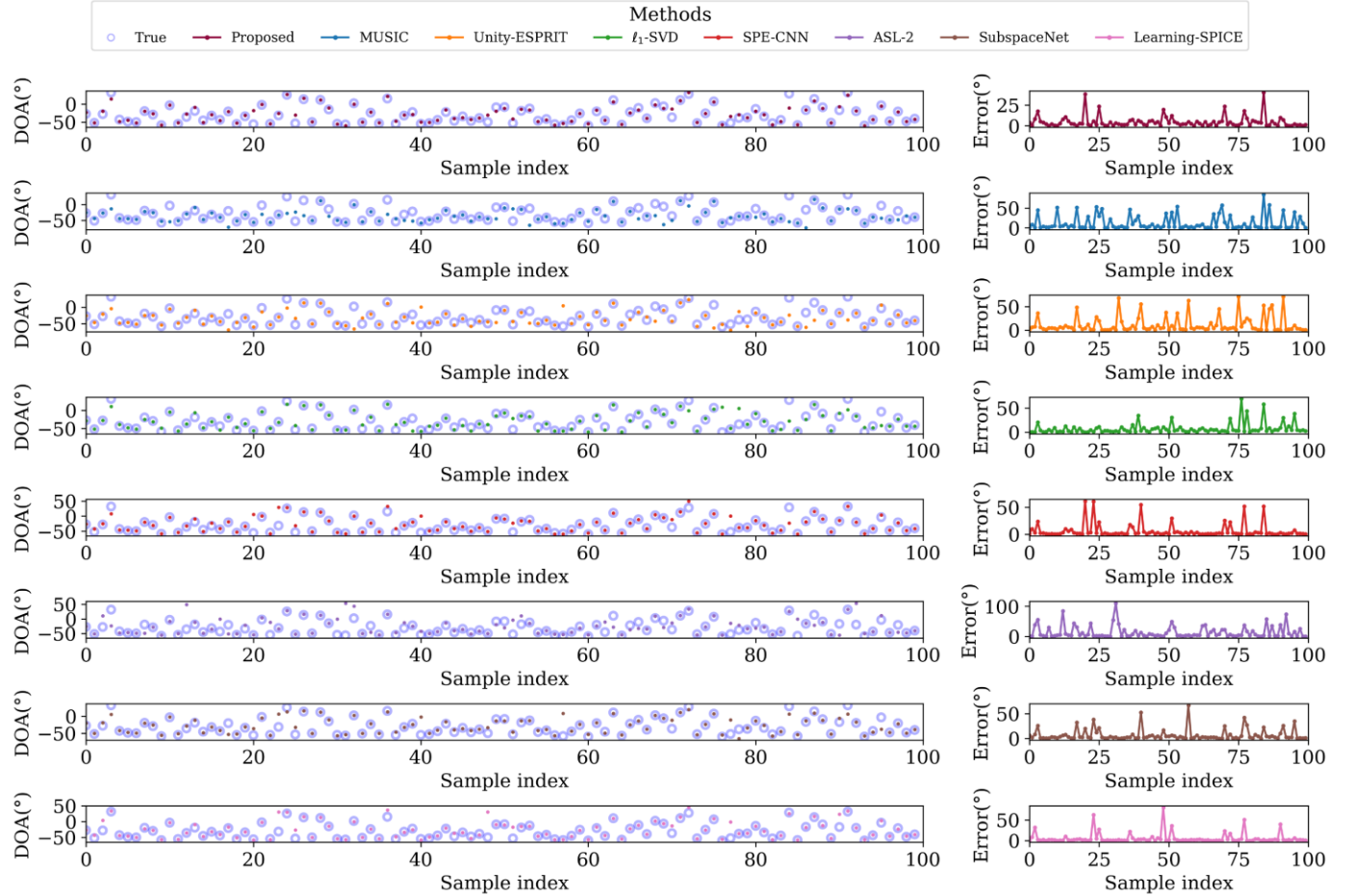


Fig. 3. DOA estimation under Scenarios 1 with $\text{SNR} = -5\text{dB}$ and $\text{snap} = 10$. Three incident signals are generated and we focus on the first one. The points represent the estimated DOA while the circles denote the true DOAs.

Table 1. CDF-Based Statistical Evaluation results under Scenarios 1 with $\text{snap} = 10$ and $\text{SNR} = -5\text{dB}$.

Algorithms	Ours	MUSIC	Unity-ESPRIT	ℓ_1 -SVD	SPE-CNN	ASL-2	SubspaceNet	Learning-SPICE
CDF(3)	55.36%	54.10%	48.90%	44.30%	60.11%	33.49%	52.63%	68.08%
CDF(10)	89.20%	73.43%	80.31%	82.93%	81.35%	55.68%	87.35%	87.51%
CDF _{10%}	0.455°	0.410°	0.526°	0.638°	0.368°	0.766°	0.501°	0.309°
CDF _{90%}	10.63°	38.13°	24.22°	20.91°	29.66°	55.20°	13.55°	16.94°

across varying array geometries and both 1D and 2D localization tasks.

In addition, the developed DOA-ViT model is trained through the Adam optimizer with a learning rate of 0.0001. The momentum parameters of the optimizer are set to $\beta_1 = 0.9$ and $\beta_2 = 0.999$, which have been shown to perform effectively in a wide range of deep learning applications. The model is trained for up to 500 epochs. To prevent overfitting and reduce training time, an early stopping strategy is employed: if the validation loss does not improve for 30 consecutive epochs, training is terminated.

For consistency and fairness, all deep learning-based baseline models are trained using the same dataset, optimizer configuration, and training strategy. This ensures a fair

comparison across different methods under identical experimental conditions.

Further implementation details, including model architecture, parameter configurations, and training scripts, are available in our open-source repository, providing full transparency and reproducibility of the experimental setup.

B. DOA estimation performance based on ViT model

To validate the effectiveness of the proposed ViT model, we first evaluate its performance in Scenario 1 through a series of targeted experiments.

Visual Performance Demonstration: To visually compare the performance of various algorithms in Scenario 1 under low SNR and limited snapshots, we present the DOA estimation results in Fig. 3, where the SNR is set to -5 dB and the number of snapshots is limited to 10. The right-hand plot in the figure

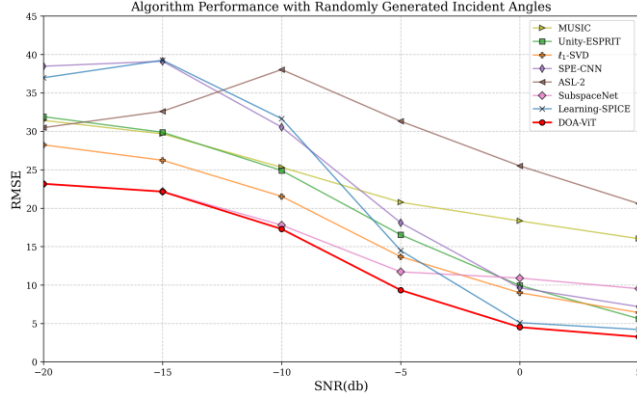


Fig. 4. RMSE vs. SNR results under Scenarios 1 with $snap = 10$. The incident signal's DOA values are randomly generated with the minimum angular interval set to 3° .

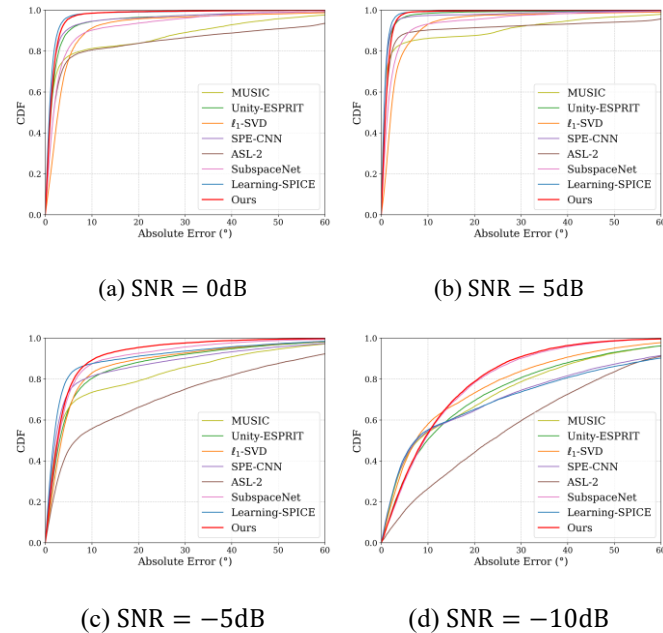


Fig. 5. CDF of the absolute error under Scenarios 1 with $snap = 10$ and various SNR, for (a) $SNR = 0dB$, (b) $SNR = 5dB$, (c) $SNR = -5dB$ and (d) $SNR = -10dB$.

depicts the absolute angular error of each method. As illustrated, the proposed method demonstrates superior performance, with most estimation errors remaining below 25° , whereas all other algorithms suffer from severe deviations, with absolute errors exceeding 50° .

RMSE vs. SNR: To evaluate the statistical performance of the model, we report the Root Mean Squared Error (RMSE) of the estimated DOA values under varying SNR conditions. As shown in Fig. 4, the RMSE versus SNR results are obtained from 5,000 Monte Carlo simulations. The proposed method consistently achieves the best performance when the incident angles are randomly generated, which can be regarded as the most general case. Learning-SPICE closely approaches the performance of the proposed model as SNR increases (SNR =

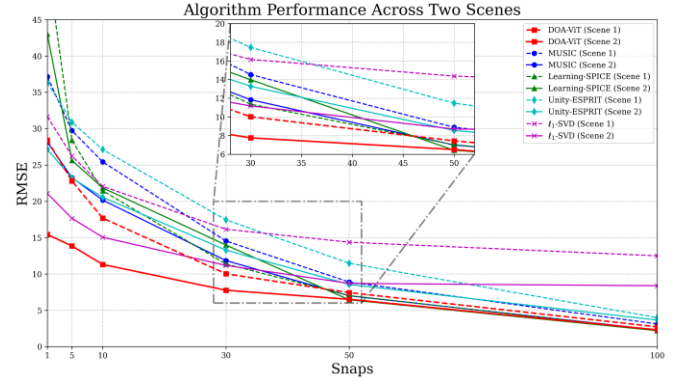


Fig. 6. RMSE vs. SNR results under Scenarios 1 with $snap = 10$. The dashed line in the figure represents Scene 1, while the solid line represents Scene 2. In Scene 1, the true DOA values are $[10^\circ, 13^\circ, 16^\circ]$, and in Scene 2, the true DOA values are $[10^\circ, 20^\circ, 30^\circ]$.

0dB or $SNR=5dB$). Unity-ESPRIT and SPE-CNN perform relatively well at high SNRs, while SubspaceNet achieves better results in low SNR scenarios. ℓ_1 -SVD exhibits stable performance, whereas MUSIC and ASL-2 exhibit inferior performance compared with the aforementioned algorithms.

Statistical Performance Evaluation: To further illustrate the statistical behavior of the model and provide a more comprehensive evaluation, the cumulative distribution function (CDF) of the absolute DOA estimation error is plotted in Fig. 5. This analysis is based on 5,000 simulation trials conducted under each condition, where the incident DOA angles are randomly generated with a minimum angular separation of 3° . The CDF provides insight into the error distribution, highlighting the robustness and accuracy of the proposed method compared to other approaches.

Through the CDF, it can be observed that under higher SNR conditions (e.g., $SNR = 0dB$ or $5dB$), the proposed model, Unity-ESPRIT, SPE-CNN and Learning-SPICE exhibit commendable performance. However, compared with other algorithms, the proposed model exhibits a lower cumulative probability of small absolute errors, and it shows a distinct advantage in larger absolute error ranges. This trend is more pronounced in low SNR scenarios like $SNR \leq 0dB$, as detailed in the following analysis.

A representative case is depicted in Fig. 5 (c), where the proposed model exhibits a slightly lower probability of absolute errors within the range of 0° to 3° compared with Learning-SPICE, SPE-CNN and MUSIC, while exhibiting advantage over the SubspaceNet, Unity-ESPRIT, ℓ_1 -SVD and ASL-2 algorithms. More notably, the probability of absolute errors of the proposed model exceeding 10° is substantially lower, which indicates a reduced frequency of high-error occurrences, highlighting our model's superior robustness relative to other approaches.

Furthermore, several statistical indicators can be derived from the CDF to quantitatively evaluate model performance. For instance, $CDF_{50\%}$ represents the absolute error corresponding to a cumulative probability of 50%, serving as a quantile-based measure of estimation accuracy. As a quantile-based measure of absolute error, it differs from the commonly used mean absolute error (MAE), which represents the mean of absolute errors; both serve as statistical measures of absolute error and

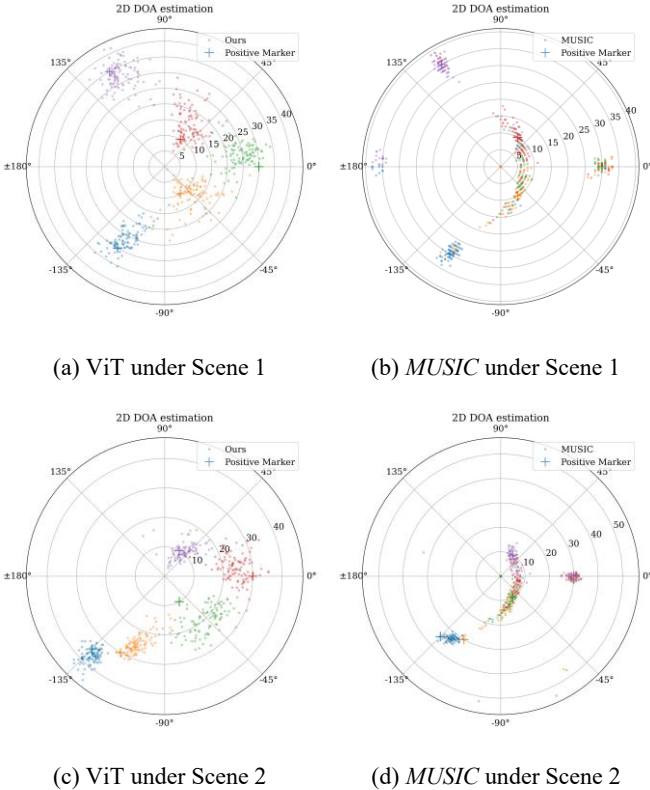


Fig. 7. Scatter plots of our proposed model and MUSIC algorithm under Scenarios 2 with $snap = 50$ and $SNR = -5\text{dB}$. Scene 1 is configured with $\boldsymbol{\theta} = [-120^\circ, -60^\circ, 0^\circ, 60^\circ, 120^\circ]$ and the corresponding azimuth angles $\boldsymbol{\phi} = [30^\circ, 10^\circ, 30^\circ, 10^\circ, 35^\circ]$. Scene 2 is configured with $\boldsymbol{\theta} = [-135^\circ, -120^\circ, -60^\circ, 0^\circ, 60^\circ]$, $\boldsymbol{\phi} = [35^\circ, 30^\circ, 10^\circ, 30^\circ, 10^\circ]$.

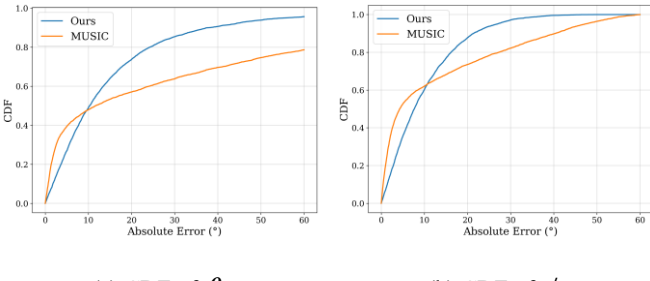


Fig. 8. The CDF of the absolute error under Scenarios 2 with $snap = 50$ and $SNR = -5\text{dB}$ is shown for: (a) $\boldsymbol{\theta}$, and (b) $\boldsymbol{\phi}$. The angles of the incident signals are randomly generated.

hold statistical significance. Similarly, $CDF(5)$ refers to the probability that the absolute error is less than 5, which can also reflect the performance of the model.

The CDF-based statistical evaluation for various models is summarized in Table 1. It can be seen that, Learning-SPICE achieves the highest DOA estimation accuracy at $CDF(3)$ and $CDF_{10\%}$, indicating a higher likelihood of producing estimates close to the true DOA. In contrast, the proposed model outperforms others at $CDF(10)$ and $CDF_{90\%}$, indicating superior robustness through a reduced incidence of large estimation errors.

RMSE vs. snapshots: To further demonstrate the performance of the model under varying snapshots and angular ranges for a ULA, we conduct experiments in different snapshot scenarios. Similar to the previous experiment, we empirically evaluate the RMSE by averaging over 5,000 Monte Carlo trials. Two distinct scenarios are considered to investigate the performance of the model under different angular ranges. Similar to the previous analysis, the root mean square error (RMSE) is computed by averaging the results over 5,000 Monte Carlo trials. Two distinct angular configurations are considered to assess the model's performance:

- Scene 1: Incident angles at $[5.1^\circ, 30.3^\circ, 54.5^\circ]$
- Scene 2: Incident angles at $[-9.9^\circ, 15.3^\circ, 39.5^\circ]$

In both scenes, the angular spacing between sources is consistent, thus the super-resolution requirement is relaxed. However, due to the broader angular span in Scene 2, the effective angular resolution is lower, which adversely affects algorithmic performance.

As shown in Fig. 6, a clear trend can be observed: for any given algorithm, the performance in Scene 1 is inferior to that in Scene 2, which can be attributed to the more challenging conditions in Scene 1. Furthermore, the proposed DOA-ViT model generally outperforms the other algorithms in this low SNR scenario. In Scene 1, our model achieves the best performance, surpassing the results achieved by MUSIC, ℓ_1 -SVD, Learning-SPICE, and Unity-ESPRIT. In Scene 2, the proposed model also attains the best performance, slightly outperforming the Learning-SPICE algorithm. These findings underscore the robustness and superior accuracy of the proposed method across varying snapshot and angular configurations.

2D DOA Estimation Performance: To evaluate the ability of the model in 2D scenarios, we expand the model by simultaneously regressing the values of $\boldsymbol{\theta}$ and $\boldsymbol{\phi}$. Two distinct scenes with varying angular separations are considered to evaluate the resolution and robustness of the model. In practical applications, it is uncommon to simultaneously vary the separations of all incident signals; therefore, only one angular parameter is altered between the two scenes to isolate its effect.

- Scene 1: The sources are configured with azimuth angle $\boldsymbol{\theta} = [-120^\circ, -60^\circ, 0^\circ, 60^\circ, 120^\circ]$ and corresponding elevation angles $\boldsymbol{\phi} = [30^\circ, 10^\circ, 30^\circ, 10^\circ, 35^\circ]$.
- Scene 2: The configuration is modified to $\boldsymbol{\theta} = [-135^\circ, -120^\circ, -60^\circ, 0^\circ, 60^\circ]$ and $\boldsymbol{\phi} = [35^\circ, 30^\circ, 10^\circ, 30^\circ, 10^\circ]$, effectively moving the fifth source closer to the first in angular space.

A representative visualization of the results is presented in Fig. 7, which facilitates an intuitive comparison of the performance of the methods. The symbol "+" represents the true location of the target, while the dot in the figure represents the predicted value of the algorithm. Each predicted value shares the same color as its corresponding ground truth for clarity. 100 Monte Carlo simulations are conducted for each scene.

According to the experimental results in Scene 1, it can be observed that the predicted results of the proposed model are predominantly clustered around the true values. In contrast, the MUSIC algorithm achieves better DOA estimation performance at the more widely separated targets, like $\boldsymbol{\theta} = [-120^\circ, +120^\circ]$ and $\boldsymbol{\phi} = [30^\circ, 35^\circ]$, but it tends to confuse the

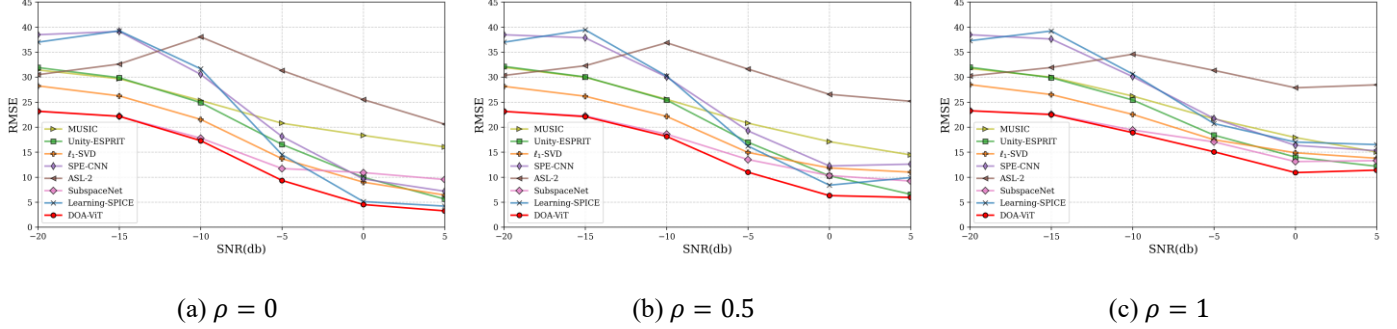


Fig. 9. Three different levels of array imperfections are proposed to evaluate the performance of DOA estimation algorithms: (a) $\rho = 0$, no array imperfections, (b) $\rho = 0.5$, moderate array imperfections, and (c) $\rho = 1$, severe array imperfections.

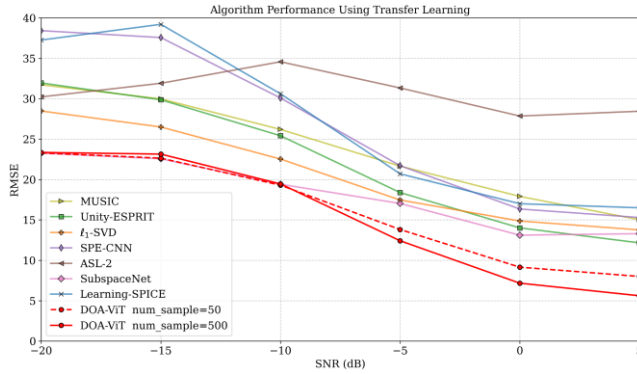


Fig. 10. RMSE vs. SNR results under Scenarios 1 with $snap = 50$ and array imperfections of $\rho = 1$. The dashed line represents the case where only 50 samples are used for transfer learning, while the solid line indicates the use of 500 samples.

other three points, resulting in poorer prediction performance. In Scene 2, we move the fifth target from $\theta = 120^\circ$, $\phi = 35^\circ$ to $\theta = -135^\circ$, $\phi = 35^\circ$, which is adjacent to the first target. In this more challenging setting, the MUSIC algorithm fails to resolve the two closely spaced targets, producing a single merged spectral peak. In contrast, the proposed model maintains high resolution, with predicted values still well clustered around their respective ground truth positions. These results highlight the superior capability of the model in achieving fine-grained localization in complex 2D DOA estimation tasks.

To further evaluate the statistical performance of the proposed model, 1,000 simulation trials are conducted, and the CDF results for each method are plotted in Fig. 8. It can be observed that the MUSIC algorithm performs better on $CDF(10)$. However, its performance deteriorates on $CDF(30)$. This suggests that while the MUSIC algorithm is likely to achieve more accurate DOA estimations for certain targets, it also shows a higher probability of producing significant DOA estimation errors. In contrast, the proposed model demonstrates a more consistent overall stability in its predictions. This experiment also demonstrates that the CDF of absolute error serves as an effective metric in DOA estimation tasks. Compared with RMSE, which is supported by the Cramér-Rao bound as its theoretical benchmark and offers a significant reference value, the CDF provides a more comprehensive assessment of the capabilities of the model. While the proposed

Table 2. Transfer Learning with Varying Sample Numbers

Sample Number	20	50	100	200
Directly Train	23.03	23.44	23.04	23.03
Fine-tune	14.17	14.38	13.57	13.84
Transfer Learning	13.66	13.27	13.06	12.72
Sample Number	300	500	800	1000
Directly Train	23.00	14.43	23.00	22.87
Fine-tune	13.30	12.79	13.31	12.38
Transfer Learning	12.60	12.54	12.21	11.48

model shows a clear advantage in terms of RMSE, the CDF analysis reveals certain limitations in its fine-grained estimation accuracy.

C. Transfer Learning Approach for Array imperfection

The presence of array imperfections introduces inconsistencies between the received signal model and the ideal model, leading to a degradation in the DOA estimation performance of the model. Scenarios involving multiple array imperfections, particularly under low SNR and small snapshot conditions, are inherently complex and challenging to handle. In this section, we demonstrate the effectiveness of the proposed transfer learning approach in these scenarios through two experiments.

1) *Transfer Learning in Scenario 1*: To evaluate the impact of array imperfections on deep learning models, we illustrate the performance of the model under scenarios involving multiple imperfections, as shown in Fig. 9. These imperfections include position bias, amplitude and phase inconsistency, and mutual coupling, with their overall severity controlled by a hyperparameter ρ . As depicted in Fig. 9, the statistical performance of both data-driven and model-driven methods deteriorates noticeably with increasing array imperfections. Although the proposed model achieves optimal performance under the ideal signal model, its performance significantly degrades when subjected to array imperfections. This degradation becomes particularly pronounced in scenarios with relatively higher SNR. When $\rho = 1$, the performance of the proposed model declines at a level similar to that of the traditional algorithms at $\rho = 0$.

To validate the effectiveness of the transfer learning approach, we evaluate the performance of the model adapted through transfer learning under varying SNR through 5,000 Monte Carlo simulations. As shown in Fig. 10, the proposed model

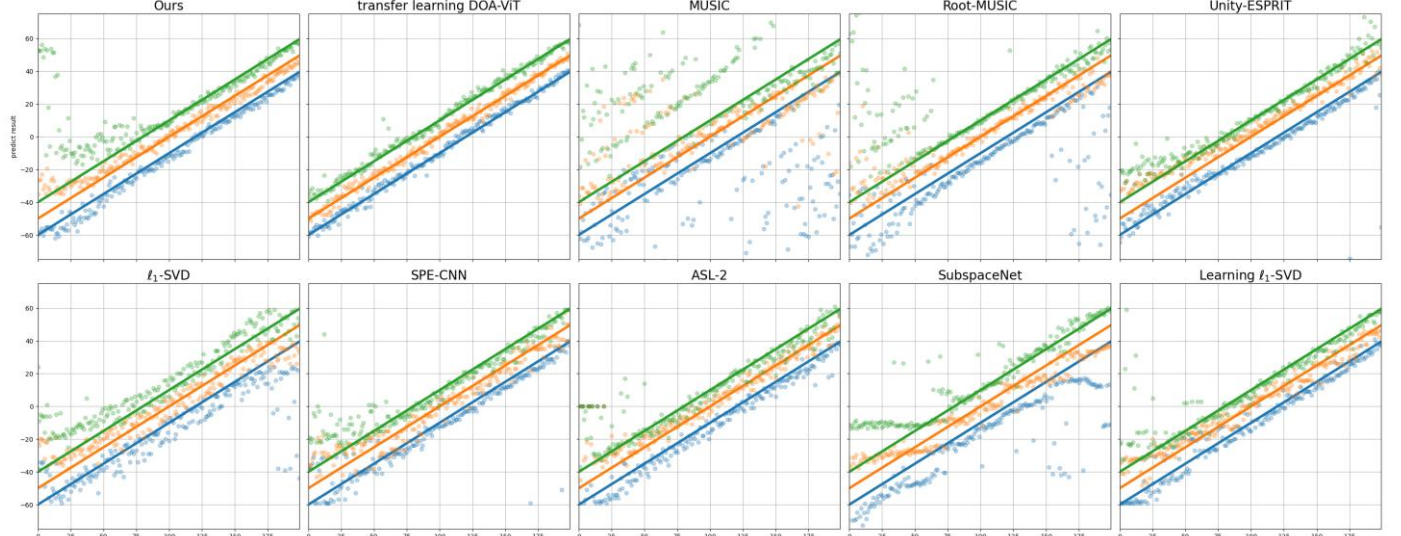


Fig. 11. DOA estimation under Scenarios 1 with $\text{SNR} = 5\text{dB}$ and $\text{snap} = 10$, $\rho = 1$. Three incident signals are generated and the interval is set to $\Delta\theta = 10^\circ$. The line represents the true location of the target, while the dot in the figure represents the predicted value of the algorithm. Additionally, the model's predicted values and their corresponding true values are marked with the same color.

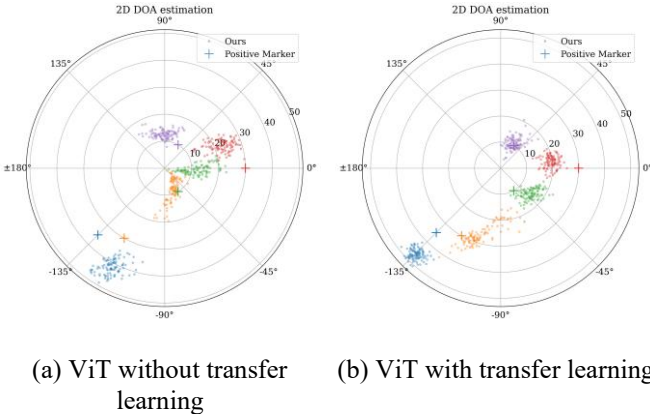


Fig. 12. DOA estimation under Scenarios 1 with $\text{SNR} = 5\text{dB}$, $\text{snap} = 10$ and array imperfections of $\rho = 1$. 100 Monte-Carlo simulations are conducted and the incident signal is configured with $\theta = [-135^\circ, -120^\circ, -60^\circ, 0^\circ, 60^\circ]$ and $\phi = [35^\circ, 30^\circ, 10^\circ, 30^\circ, 10^\circ]$.

achieves significant improvement even with only 50 samples, demonstrating accurate DOA estimation under low SNR and small snapshot scenarios. Moreover, when more samples (500 samples) are used, the performance of the model is further enhanced.

Furthermore, to demonstrate the superiority of the proposed transfer learning algorithm, a comparison experiment is carried out under Scenario 1 with $\text{snap} = 10$, $\text{SNR} = -5\text{dB}$, and array imperfections $\rho = 1$. Our method is compared with two baseline approaches: (1) directly training the model through the samples with array imperfections (Directly Train), and (2) fine-tuning the model pre-trained on simulated data (Fine-tune). The performance of these three methods is evaluated across varying numbers of array imperfection samples, as shown in Table 2. The results indicate that the proposed transfer learning algorithm consistently achieves superior performance in most cases. This demonstrates that a well-designed transfer learning

strategy can more effectively leverage limited sample information, leading to superior performance compared to other methods.

Fig. 11 illustrates the performance of the proposed model after transfer learning. From the experimental results, it can be observed that the proposed model exhibits significant bias before applying transfer learning, particularly when the incident angles are close to -60° . However, after applying transfer learning, the predict results of the proposed model become concentrated around the true values. In contrast, due to the combined effects of multiple array imperfections, MUSIC and ℓ_1 -SVD show large deviations, while Unity-ESPRIT and SPE-CNN suffer from performance degradation when the incident angles span a wider range. SubspaceNet exhibits noticeable distortions, failing to achieve accurate DOA estimation. Learning-SPICE, SPE-CNN and ASL-2 demonstrate enhanced resilience to array imperfections; however, systematic distortion remains observable in the predict results.

2) *Transfer Learning in Scenario 2*: To further validate the effectiveness of the proposed transfer learning algorithm, we extend the algorithm to 2D DOA estimation. As shown in Fig. 12; it can be clearly observed that prior to the application of the transfer learning algorithm, the model fails to effectively distinguish between the first target ($\theta = -135^\circ, \phi = 35^\circ$) and the second target ($\theta = -120^\circ, \phi = 30^\circ$) and exhibits significant bias for other targets due to array imperfections. However, after the transfer learning algorithm is applied, the prediction bias is substantially corrected, and the predicted values are able to converge near the true target.

VI. CONCLUSION

In this work, we develop a DOA-ViT model for DOA estimation, which leverages the attention mechanism to capture global dependencies. By directly learning the mapping from the sampled SCM to DOA values, the proposed method can be easily extended to arbitrary array geometries or 2D DOA estimation scenarios, demonstrating strong adaptability.

Extensive simulations are conducted to evaluate the performance and robustness of the proposed model.

Furthermore, deep learning based DOA estimators often suffer from severe performance degradation in practical scenarios with array imperfections. To overcome this limitation, we propose a supervised transfer learning strategy to mitigate the performance degradation in practical scenarios. By aligning the features of the source and target domains in a supervised manner, the proposed method demonstrates improved results in practical scenarios with array imperfections.

It is worth noticing that this work is the first to introduce an advanced transfer learning strategy to address array imperfections. Investigating how to effectively leverage transfer learning methods to improve the performance of deep learning models in scenarios with array imperfections is a significant and worthwhile research direction, and has the potential to enhance the performance of deep learning algorithms in practical applications. Further exploration of various transfer learning approaches for handling array imperfections is encouraged.

ACKNOWLEDGMENT

The authors would like to thank the anonymous reviewers for their insightful comments and suggestions.

REFERENCES

- [1]. G. Papageorgiou, M. Sellathurai, and Y. Eldar, “Deep networks for direction-of-arrival estimation in low SNR,” *IEEE Transactions on Signal Processing*, vol. 69, no. 6, pp. 3714–3729, Jun. 2021.
- [2]. M. Wang, F. Gao, S. Jin, and H. Lin, “An overview of enhanced massive MIMO with array signal processing techniques,” *IEEE Journal of Selected Topics in Signal Processing*, vol. 13, no. 5, pp. 886–901, Sep. 2019.
- [3]. K. Xu, X. Xia, C. Li, W. Xie, J. Liu, R. Zhu, and H. He, “Robust DOA estimation and tracking for integrated sensing and communication massive MIMO OFDM systems,” *Science China Information Sciences*, vol. 66, no. 10, p. 202302, Nov. 2023.
- [4]. W. Zhang, P. Wang, N. He, and Z. He, “Super resolution DOA based on relative motion for FMCW automotive radar,” *IEEE Transactions on Vehicular Technology*, vol. 69, no. 8, pp. 8698–8709, Aug. 2020.
- [5]. R. Akter, V. S. Doan, T. Huynh-The, and D. S. Kim, “RFDOA-Net: an efficient ConvNet for RF-based DOA estimation in UAV surveillance systems,” *IEEE Transactions on Vehicular Technology*, vol. 70, no. 11, pp. 12209–12214, Nov. 2021.
- [6]. C. Huang, Z. Tian, K. Liu, and J. Xu, “DoA estimation via sparse bayesian learning in a non-cooperative mode using a single RF link,” in *Proc. GLOBECOM 2024 - 2024 IEEE Global Communications Conference*, Cape Town, South Africa, pp. 2617–2622, Dec. 2024.
- [7]. X. Song, G. Ding, Y. Xu, H. Wang, J. Gu, and Y. Liu, “Cooperative sensing of non-cooperative beam signals,” *IEEE Transactions on Cognitive Communications and Networking*, vol. 10, no. 3, pp. 807–818, Jun. 2024.
- [8]. N. Wang, P. Agathoklis, and A. Antoniou, “A new DOA estimation technique based on subarray beamforming,” *IEEE Transactions on Signal Processing*, vol. 54, no. 9, pp. 3279–3290, Sep. 2006.
- [9]. M. Haardt and J. A. Nossek, “Unitary ESPRIT: how to obtain increased estimation accuracy with a reduced computational burden,” *IEEE Transactions on Signal Processing*, vol. 43, no. 5, pp. 1232–1242, May 1995.
- [10]. R. Schmidt, “Multiple emitter location and signal parameter estimation,” *IEEE Transactions on Antennas and Propagation*, vol. 34, no. 3, pp. 276–280, Mar. 1986.
- [11]. A. Barabell, “Improving the resolution performance of eigenstructure-based direction-finding algorithms,” in *Proc. ICASSP '83. IEEE International Conference on Acoustics, Speech, and Signal Processing*, Boston, MASS, USA, pp. 336–339, Apr. 1983.
- [12]. F. G. Yan, L. Shuai, J. Wang, J. Shi, and M. Jin, “Real-valued root-MUSIC for DOA estimation with reduced-dimension EVD/SVD computation,” *Signal Processing*, vol. 152, pp. 1–12, Nov. 2018.
- [13]. S. Qiu, W. Sheng, X. Ma, and T. Kirubarajan, “A maximum likelihood method for joint DOA and polarization estimation based on manifold separation,” *IEEE Transactions on Aerospace and Electronic Systems*, vol. 57, no. 4, pp. 2481–2500, Aug. 2021.
- [14]. M. Meller and K. Stawiarski, “On DoA estimation for rotating arrays using stochastic maximum likelihood approach,” *IEEE Transactions on Signal Processing*, vol. 68, no. 9, pp. 5219–5229, Sep. 2020.
- [15]. P. Forster, P. Larzabal, and E. Boyer, “Threshold performance analysis of maximum likelihood DOA estimation,” *IEEE Transactions on Signal Processing*, vol. 52, no. 11, pp. 3183–3191, Nov. 2004.
- [16]. D. Malioutov, M. Cetin, and A. S. Willsky, “A sparse signal reconstruction perspective for source localization with sensor arrays,” *IEEE Transactions on Signal Processing*, vol. 53, no. 8, pp. 3010–3022, Aug. 2005.
- [17]. Z. Yang and L. Xie, “Enhancing sparsity and resolution via reweighted atomic norm minimization,” *IEEE Transactions on Signal Processing*, vol. 64, no. 4, pp. 995–1006, Feb. 2016.
- [18]. Z. M. Liu, Z. T. Huang, and Y. Y. Zhou, “An efficient maximum likelihood method for direction-of-arrival estimation via sparse bayesian learning,” *IEEE Transactions on Wireless Communications*, vol. 11, no. 10, pp. 1–11, Oct. 2012.
- [19]. P. Stoica, P. Babu, and J. Li, “SPICE: a sparse covariance-based estimation method for array processing,” *IEEE Transactions on Signal Processing*, vol. 59, no. 2, pp. 629–638, Feb. 2011.
- [20]. N. D. M. Rondel and G. Y. Burel, “Cooperation of multi-layer perceptrons for angles of arrival estimation,” in *Proc. 4th International Conference on Artificial Neural Networks*, Cambridge, UK, pp. 323–328, Jun. 1995.
- [21]. Y. M. Wang and Y. L. Ma, “The performance of neural network for high resolution direction-of-arrival estimation,” in *Proc. 1991 International Conference on Circuits and Systems*, Shenzhen, China, pp. 301–304, Jun. 1991.
- [22]. Y. Kase, T. Nishimura, T. Ohgane, Y. Ogawa, D. Kitayama, and Y. Kishiyama, “DOA estimation of two targets with deep learning,” in *Proc. 2018 15th Workshop on Positioning, Navigation and Communications (WPNC)*, Bremen, Germany, pp. 1–5, Oct. 2018.
- [23]. Z. M. Liu, C. Zhang, and P. S. Yu, “Direction-of-arrival estimation based on deep neural networks with robustness to array imperfections,” *IEEE Transactions on Antennas and Propagation*, vol. 66, no. 12, pp. 7315–7327, Dec. 2018.
- [24]. Z. Zhao and J. Li, “DoA estimation based on deep learning in low SNR,” in *Proc. 2023 IEEE International Symposium on Broadband Multimedia Systems and Broadcasting (BMSB)*, Beijing, China, pp. 1–4, Jun. 2023.
- [25]. Z. W. Tan, Y. Liu, and A. W. H. Khong, “A dilated inception convolutional neural network for gridless DOA estimation under low SNR scenarios,” in *Proc. 2022 Asia-Pacific Signal and Information Processing Association Annual Summit and Conference (APSIPA ASC)*, Chiang Mai, Thailand, pp. 760–764, Nov. 2022.
- [26]. X. Wu, X. Yang, X. Jia, and F. Tian, “A gridless DOA estimation method based on convolutional neural network with toeplitz prior,” *IEEE Signal Processing Letters*, vol. 29, pp. 1247–1251, May 2022.
- [27]. H. Xiang, B. Chen, M. Yang, and S. Xu, “Angle separation learning for coherent DOA estimation with deep sparse prior,” *IEEE Communications Letters*, vol. 25, no. 2, pp. 465–469, Feb. 2021.
- [28]. S. Xu, A. Brighente, B. Chen, M. Conti, X. Cheng, and D. Zhu, “Deep neural networks for direction of arrival estimation of multiple targets with sparse prior for line-of-sight scenarios,” *IEEE Transactions on Vehicular Technology*, vol. 72, no. 4, pp. 4683–4696, Apr. 2023.
- [29]. D. H. Shmuel, J. P. Merkofer, G. Revach, R. J. G. Van Sloun, and N. Shlezinger, “SubspaceNet: deep learning-aided subspace methods for DoA estimation,” *IEEE Transactions on Vehicular Technology*, vol. 74, no. 3, pp. 4962–4976, Mar. 2025.
- [30]. Y. LeCun, Y. Bengio, and G. Hinton, “Deep learning,” *Nature*, vol. 521, no. 7553, pp. 436–444, May 28, 2015.
- [31]. B. Allen and M. Ghavami, *Adaptive array systems: fundamentals and applications*, John Wiley & Sons, 2005.
- [32]. S. Liu, Z. Zhang, and Y. Guo, “2-D DOA estimation with imperfect L-shaped array using active calibration,” *IEEE Communications Letters*, vol. 25, no. 4, pp. 1178–1182, Apr. 2021.

- [33]. B. C. Ng and C. M. S. See, "Sensor-array calibration using a maximum-likelihood approach," *IEEE Transactions on Antennas and Propagation*, vol. 44, no. 6, pp. 827–835, Jun. 1996.
- [34]. K. V. Stavropoulos and A. Manikas, "Array calibration in the presence of unknown sensor characteristics and mutual coupling," in *Proc. 10th European Signal Processing Conference*, Tampere, Finland, pp. 1–4, Sep, 2000.
- [35]. M. Zhang and Z. D. Zhu, "Array shape calibration using sources in known directions," in *Proc. IEEE 1993 National Aerospace and Electronics Conference-NAECON 1993*, Dayton, OH, USA, pp. 70–73, May 1993.
- [36]. B. C. Ng and A. Nehorai, "Active array sensor localization," *Signal Processing*, vol. 44, no. 3, pp. 309–327, Jul. 1995.
- [37]. Z. M. Liu and Y. Zhou, "A unified framework and sparse Bayesian perspective for direction-of-arrival estimation in the presence of array imperfections," *IEEE Transactions on Signal Processing*, vol. 61, no. 15, pp. 3786–3798, Aug. 2013.
- [38]. X. Zhang, Z. He, X. Zhang, and Y. Yang, "DOA and phase error estimation for a partly calibrated array with arbitrary geometry," *IEEE Transactions on Aerospace and Electronic Systems*, vol. 56, no. 1, pp. 497–511, Feb. 2020.
- [39]. A. Liu, G. Liao, C. Zeng, Z. Yang, and Q. Xu, "An eigenstructure method for estimating DOA and sensor gain-phase errors," *IEEE Transactions on Signal Processing*, vol. 59, no. 12, pp. 5944–5956, Dec. 2011.
- [40]. K. Han, P. Yang, and A. Nehorai, "Calibrating nested sensor arrays with model errors," *IEEE Transactions on Antennas and Propagation*, vol. 63, no. 11, pp. 4739–4748, Nov. 2015.
- [41]. F. Sellone and A. Serra, "A novel online mutual coupling compensation algorithm for uniform and linear arrays," *IEEE Transactions on Signal Processing*, vol. 55, no. 2, pp. 560–573, Feb. 2007.
- [42]. Z. Ye and C. Liu, "On the resiliency of MUSIC direction finding against antenna sensor coupling," *IEEE Transactions on Antennas and Propagation*, vol. 56, no. 2, pp. 371–380, Feb. 2008.
- [43]. Z. Liu, Z. Huang, F. Wang, and Y. Zhou, "DOA estimation with uniform linear arrays in the presence of mutual coupling via blind calibration," *Signal Processing*, vol. 89, no. 7, pp. 1446–1456, Jul. 2009.
- [44]. K. Weiss, T. M. Khoshgoftaar, and D. Wang, "A survey of transfer learning," *Journal of Big Data*, vol. 3, no. 1, pp. 1–40, May 2016.
- [45]. X. Wu, J. Wang, X. Yang, and F. Tian, "A gridless DOA estimation method based on residual attention network and transfer learning," *IEEE Transactions on Vehicular Technology*, vol. 73, no. 6, pp. 9103–9108, Jun. 2024.
- [46]. M. Zhang, C. Wang, W. Zhu, and Y. Shen, "An intelligent DOA estimation error calibration method based on transfer learning," *Applied Sciences*, vol. 12, no. 15, p. 7636, Jul. 2022.
- [47]. N. Labbaf, H. R. Dalili Oskouei, and M. R. Abedi, "Robust DoA estimation in a uniform circular array antenna with errors and unknown parameters using deep learning," *IEEE Transactions on Green Communications and Networking*, vol. 7, no. 4, pp. 2143–2152, Dec. 2023.
- [48]. B. Friedlander and A. J. Weiss, "Direction finding in the presence of mutual coupling," *IEEE Transactions on Antennas and Propagation*, vol. 39, no. 3, pp. 273–284, Mar. 1991.
- [49]. A. Dosovitskiy, L. Beyer, A. Kolesnikov, D. Weissenborn, X. Zhai, T. Unterthiner, M. Dehghani, M. Minderer, G. Heigold, S. Gelly, J. Uszkoreit, and N. Houlsby, "An image is worth 16x16 words: transformers for image recognition at scale," in *Proc. International Conference on Learning Representations*, Vienna, Austria, May 2021.
- [50]. I. Nejjar, Q. Wang, and O. Fink, "DARE-GRAM: unsupervised domain adaptation regression by aligning inverse gram matrices," in *Proc. IEEE/CVF Conference on Computer Vision and Pattern Recognition*, Vancouver, BC, Canada, pp. 11744–11754, Jun. 2023.
- [51]. B. B. Zhang, D. Zhang, Y. Li, Y. Hu, and Y. Chen, "Unsupervised domain adaptation for rf-based gesture recognition," *IEEE Internet of Things Journal*, vol. 10, no. 23, pp. 21026–21038, Dec. 2023.